Steady-State Behavior of Liquid Fuel Hydrazine Decomposition in Packed Bed

Baolin Hou, Xiaodong Wang, Tao Li, and Tao Zhang
State Key Laboratory of Catalysis, Dalian Institute of Chemical Physics, Chinese Academy of Sciences, Dalian 116023, China

DOI 10.1002/aic.14703
Published online December 11, 2014 in Wiley Online Library (wileyonlinelibrary.com)

A general theoretical model is presented to analyze the steady-state decomposition process of liquid monopropellants in packed beds for thruster systems. Additionally, an experiment studying the decomposition of liquid hydrazine in a packed bed is used to validate this model. The liquid droplet evaporation rate is determined through calculating the gas-liquid mass transfer for the mixture temperatures lower than the liquid propellant boiling point and solving the gas-liquid or liquid-solid heat transfer equations at the temperature exceeding the boiling point. The process of liquid propellant decomposition in packed beds are simulated based on the Naive–Stokes equation for the mixture model integrated with the developed liquid evaporation rate, in which both the heterogeneous catalytic reaction coupled with the diffusion of reactants in the pore of catalyst, and the homogenous decomposition reactions are considered. The calculated results for the axial distribution of the temperature are in good agreement with the experimental data. © 2014 American Institute of Chemical Engineers *AIChE J*, 61: 1064–1080, 2015

Keywords: liquid propellant decomposition, packed bed, porous media, gas-liquid two-phase flow, liquid droplet evaporation, monopropellant

Introduction

The monopropellant thruster system is widely used to adjust the orbit of and control the attitude of satellites and spacecraft in space missions. Hydrogen peroxide was first developed as a monopropellant by Germany.[1] Due to the low specific impulse (in the range of 165–185 s) of monopropellant hydrogen peroxide,[2] it was gradually replaced by hydrazine (specific impulse 220 s) after hydrazine and Shell 405 catalyst developed. Recently, with the satellite evolution directed toward single-function microsatellites, hydrogen peroxide received some researchers' attention again in the microthrusters system.[3–9] However, due to being simple and reliable,[10–12] the decomposition of hydrazine in packed beds is still widely used in monopropellant thruster systems in the common spacecraft. In addition, considering the toxicity of hydrazine-based propellant and the low specific impulse of hydrogen peroxide, some aqueous energetic ionic liquids, such as ammonium dinitramide (ADN), hydroxyl ammonium nitrate, and hydrazinium nitroformate, have been proposed and investigated as new monopropellants.[13–20] Although some experiments investigating these green monopropellants have been developed in the laboratory, due to some engineering problems, these new monopropellants are not widely used in practice. The hydrazine-based monopropellant thruster system is still one of main sources of power in space missions because of its high reliability. Therefore, in this article, liquid hydrazine decomposition in packed beds is theoretically and experimentally investigated. In addition, the model developed in this article constitutes a general theory that can be used to analyze other monopropellant thruster system by simple replacing the relevant chemical reaction kinetic parameters and propellant property parameters.

In the hydrazine-based monopropellant thruster system, hydrazine can spontaneously decompose into ammonia, hydrogen, and nitrogen in the presence of metal catalysts such as iridium at relatively low temperatures, through which chemical energy is converted into dynamic energy, and then propulsion force is produced. Although this process has been applied to thruster systems for many decades, a clear understanding of this process is still lacking due to its fast reaction rate and the toxicity of hydrazine, which make these system quite difficult to investigate in detail through experimental methods. To enhance the effectiveness for designing and developing such propellant systems, numerical simulations have often been used to analyze and understand the effects of various design and operational parameters on the performance of thruster systems.[21,22]

In a previous study, Kesten[23] first formulated a numerical method to analyze the steady-state and transient behavior for the catalytic decomposition of liquid hydrazine in a packed bed. In his model, the resistance to the intraparticle diffusion of the reactants, the gas-solid mass transfer and heat transfer, and the conservation of mass and energy were considered. Kesten[23] also extended his model to allow for varying feed pressure and mass flow rate with times by simply

Additional Supporting Information may be found in the online version of this article.

Corresponding concerning this article should be addressed to X. Wang at xdwang@dicp.ac.cn.

considering the reaction chamber fluid dynamics to simulate the process of the thruster start-up. With using this model, Kesten[23] obtained extensive numerical results under various operational conditions, which were validated by the relevant experimental data. As a result, Kesten's model[23] is still currently used for analyzing the process of liquid hydrazine catalytic decomposition in a packed bed.[24] However, Shankar et al.[25] thought there were some limitations in the usefulness of this model's results for designing an optimized thruster considering the correlation of numerical data. In addition, in Kesten's model[23] the transport limitations between the phases were ignored and all of the energy released by the catalytic decomposition of hydrazine in the entrance of packed bed was assumed to vaporize the liquid hydrazine.

Urrutia and Linan[26] developed an analytical model for steady-state hydrazine decomposition to circumvent the complicated numerical calculation in Kesten's model.[23] In their model, the hydrazine decomposition was divided into three distinct regions: the induction region, the two-phase region and the postinduction region. In the induction region, the only relevant decomposition is that of hydrazine, and all of the energy released is used to heat liquid hydrazine to its boiling point. When the temperature reaches the boiling point, the liquid hydrazine is then rapidly vaporized while the process continues into the two-phase region. In the two-phase region, gas and liquid coexist, and the liquid hydrazine is further vaporized. At the end of the two-phase region, a gas mixture is formed and has access to the postinduction region, where the residual hydrazine is heterogeneously and homogeneously decomposed into ammonia, hydrogen, and nitrogen; the catalytic dissolution of ammonia also occurs in the high-temperature region. Under these assumptions, the complicated physical phenomenon of the catalytic decomposition of hydrazine in a packed bed was reduced to three individual regions. Additionally, analytical expressions for the length of every region and for all of the fluid components were obtained. Therefore, the effect of each parameter on the thruster performance could be very easily evaluated. This artificial assumption simplifies the process of calculating the liquid hydrazine decomposition in a packed bed, but limits the general applicability of the model.

With the development of computational fluid dynamics (CFD) commercial software and computer technology, investigating some complicated systems including multiple physical and chemical processes, has become possible. The underlying principles of processes such as the decomposition of a liquid propellant in a packed bed characterized by high temperature and pressure, high toxicity reactants or fast reaction, which are difficult to study through the experimental method, can be clearly investigated by CFD.[27–29] Zhou[30] first used CFD tools to explore a hydrogen peroxide-based monopropellant microthruster system and to optimize the packed bed together along with designing the nozzle and thruster systems. For simplification, the authors ignored the process of heating and vaporizing the liquid, and the steam of the liquid was assumed as the inlet condition. The effect of liquid evaporation is not considered in their study, reducing the process to single-phase flow in a porous media. However, the vaporization of liquid droplet in porous media has been verified to be important for this process.[31] In addition, recently, for the numerical simulation of propellant combustion in space, Plaud et al.[32] used the direct numerical simulations to analyze the process of heterogeneous propellant combustion. Thakre et al.[33] used one–dimensional (1-D) N–S equation coupled with the detailed chemical kinetics to simulate the process of liquid ADN monopropellant burning in the space. Amri and Rezoug[34] used the thermochemical method to investigate the liquid propellants combustion for space applications. Zaseck[35] used the granular diffusion flame theory to simulate the combustion of micro aluminum and hydrogen peroxide. It is possible that these models would be used to analyze liquid monopropellants decomposition in packed beds in future.

In this article, the process of hydrazine decomposition in a packed bed is simulated by CFD methods, considering the liquid droplet vaporization in porous media. The liquid hydrazine is first injected into the packed bed through a capillary tube by high-pressure nitrogen and then atomized into droplets by atomizers at the exit of the capillary tube. When the droplets contact hot catalyst particles, the liquid hydrazine is heated and vaporized through gas-liquid and liquid-solid heat transfer; the vaporized product is catalytically decomposed, and chemical energy is released. In this situation, the fluid is accelerated from a velocity of a few millimeters per second at the entrance to a few meters per second at the exit by flowing through a packed bed of 2 to 3 cm, and it is heated from atmosphere temperature to be higher than 800°C[23]; the problem is strongly nonlinear, involving the multiple coupled physical and chemical equations. Although numerical methods have been thoroughly developed in the past, solving the equations for simulating this process using the grid N–S theories for multiphase flow in porous media is still challenging. To analyze this process with a mathematical model, some assumptions have to be made to simplify the physical and chemical process; for example, the relative gas-liquid slip in the porous media is ignored due to the strong interaction between the phases, so the gas and liquid phases can be treated as a homogeneous mixture phase in solving the momentum equations. The rate of vaporization of the liquid droplets is calculated by different models in different temperature ranges. When the mixture temperature is lower than the liquid boiling point, the corresponding value is obtained by calculating the gas-liquid mass transfer. When the mixture temperature exceeds the liquid boiling point, the process is dominated by the gas-liquid or liquid-solid heat transfer, where the relative contribution can be determined by solving the collision probability between the liquid droplet and the hot solid catalyst. For energy transport, the energy conservation equations for the mixture phase and the solid phase are solved, and the dispersion of the mixture phase from the catalyst packing structure, the thermal conductivity, and the radiation of the catalyst are considered. The gas-solid mass transfer and gas intraparticle diffusion are also taken into account for calculating the reaction rate. The models developed here are solved by the CFD software Fluent 6.3.26 with user defined scalars (UDS), user defined functions (UDF) and user defined memory (UDM). The simulation results were validated by the experimental data, which were performed in a packed bed of ID 18 mm and length 29 mm in a vacuum chamber with an absolute pressure of 0.5 Pa.

Model

The decomposition of liquid hydrazine in a packed bed involves a large number of complicated nonlinear physical and chemical processes, such as liquid vaporization, liquid phase disappearance, gas phase appearance, gas phase

diffusion and reaction, and momentum, mass and heat transfer between the gas and the solid or the gas and the liquid. In particular, the interactions among the gas, the solid, and the liquid in this system are often several orders higher than those of general chemical industrial processes. To circumvent these complications, the following assumptions have to be made:

1. The gas-liquid relative slip is ignored as a result of the strong interaction between the gas and the liquid in the porous media, so the gas and liquid can be treated as a homogeneous fluid.

2. The liquid hydrazine is assumed to be uniformly injected into the packed bed at the arbitrarily selected inlet location.

3. Because the packed bed is often used under vacuum, the effect of heat transfer at the wall boundary can be ignored. The anisotropy of the heat and mass transfer resulting from dispersion is also not considered.

4. The effect of the capillary pressure among particles is neglected, and the pressure drop of the packed bed is calculated by the semiempirical Ergun equation.

5. Because the pores among in the catalyst particles are smaller than the turbulence length scale, the effect of turbulence on the fluid viscosity is not included.

6. The reaction rate is assumed to be enough fast to prevent liquid hydrazine from wetting the pores of the particles, so only the vapor-phase reaction is considered.

7. According to Martyneko's[36] assumptions for dealing with liquid droplets burning in porous media, the interaction between droplets during evaporation is neglected, and the liquid fuel droplets are assumed to be monodisperse. Here, the mean diameter of the initial liquid droplet is characterized to be 120 μm by PDA (laser phase Doppler anemoneter).

8. According to the literature,[23] in the appropriate range of temperatures and pressures for the operation of thrusters the decomposition of hydrazine are represented as a three-step reaction mechanism:

$$2N_2H_4 \xrightarrow{\text{Cat}} 2NH_3 + N_2 + H_2$$

$$2N_2H_4 \xrightarrow{\text{Heat}} 2NH_3 + N_2 + H_2$$

$$2NH_3 \xrightarrow{\text{Cat}} N_2 + 3H_2$$

A model for liquid hydrazine decomposition in a packed bed is developed according to the above assumptions. In addition, the corresponding governing equations will be detailed in the following sections.

Mass conservation

$$\nabla \cdot (\varepsilon_b \rho_m u_m) = 0 \tag{1}$$

Here, ε_b is the porosity of the packed bed, u_m is the velocity of the mixture, and ρ_m is the mixture density, which can be calculated as:

$$\rho_m = \varepsilon_g \rho_g + \varepsilon_L \rho_L \tag{2}$$

where ε_g and ε_L are the volume fractions of the gas and the liquid, respectively. The density of the gas phase can be obtained from the ideal gas law:

$$p = \frac{\rho_m R T_m}{\overline{M_m}} \tag{3}$$

where $\overline{M_m}$ is molar average molecular weight of the mixture, T_m is the temperature of mixture, and R is the ideal gas constant.

Momentum conservation

$$\nabla \cdot (\varepsilon_b \rho_m u_m u_m) = -\varepsilon_b \nabla p + \nabla \cdot \left[\mu_m \left(\nabla u_m + \nabla u_m^T\right)\right] + S_M \tag{4}$$

Here, S_M denotes the momentum sink vector term due to the packed catalyst, which can be calculated by the well-known semiempirical Ergun equation:

$$S_M = \left[\frac{180\mu_m(1-\varepsilon_b)^2}{{d_c}^2{\varepsilon_b}^3} U_m + \frac{1.8\rho_m(1-\varepsilon_b)}{d_c{\varepsilon_b}^3} |U_m| U_m\right] \tag{5}$$

where U_m is the superficial velocity of the mixture, and d_c the diameter of catalyst. The viscosity of the mixture can be expressed as:

$$\mu_m = \mu_g \varepsilon_g + \mu_L \varepsilon_L \tag{6}$$

where μ_m, μ_g, and μ_L are the viscosities of the mixture, the gas, and the liquid, respectively.

Volume fraction of gas and liquid

According to mass conservation for the liquid phase, the liquid volume fraction equation can be written as:

$$\nabla \cdot (\varepsilon_L \varepsilon_b \rho_L u_m) = m_{g,L} \tag{7}$$

where $m_{g,L}$ is the mass exchange between the gas and the liquid. In addition, the volume fraction of gas can be described as:

$$\varepsilon_L + \varepsilon_g = 1 \tag{8}$$

Energy conservation

The energy conservation equation for the mixture can be expressed as

$$\nabla \cdot \left(\sum_{i=g,L} \varepsilon_i u_m (\rho_i E_i + p)\right) = -\nabla \cdot (\lambda_m \nabla T_m) + S_E + S_r \tag{9}$$

where λ_m is the thermal conductivity o f the mixture, which will be described in detail in the section of thermal conductivity.

$$E_i \text{ is defined as: } E_i = \begin{cases} h_L \\ h_g - \dfrac{p}{\rho_g} + \dfrac{{u_g}^2}{2} \end{cases} \tag{10}$$

where h_L and h_g are the enthalpy of the liquid and the gas, respectively, at a certain temperature.

Regarding a solid catalyst, the energy conservation equation can be written as

$$\nabla \cdot \left(k_s^e \nabla T_s\right) = -S_E \tag{11}$$

The heat source S_E represents the heat transfer between the mixture phase and the solid

$$S_E = \alpha_{m,s}(1-\varepsilon_b)\frac{6}{dp}(T_s - T_m) \tag{12}$$

where $\alpha_{m,s}$ is the heat-transfer coefficient between the mixture phase and the solid, and it can be calculated as

$$\alpha_{m,s} = 2\varepsilon_b\frac{\lambda_m}{d_c} + 0.69\frac{\lambda_m}{d_c}\left(\frac{U_m d_p \rho_m}{\varepsilon_b \mu_m}\right)^{1/2}\left(\frac{C_{p,m}\mu_m}{\lambda_m}\right)^{1/3} \tag{13}$$

In Eq. 9, the source term S_r represents the chemical reaction heat.

$$S_r = \left(R_{het}^{N_2H_4} + R_{hom}^{N_2H_4}\right)\Delta H_r^{N_2H_4} + R_{het}^{NH_3}\Delta H_r^{NH_3} \tag{14}$$

$R_{het}^{N_2H_4}$ and $R_{hom}^{N_2H_4}$ are the reaction rates of the heterogeneous and homogeneous decomposition of vapor hydrazine, respectively; $R_{het}^{NH_3}$ is the heterogeneous decomposition rate of ammonia; and $\Delta H_r^{N_2H_4}$ and $\Delta H_r^{NH_3}$ are the enthalpies of reaction for hydrazine decomposition and ammonia dissolution, respectively.

Species transport equations

Based on the theory of species conversion, the species transport equations of hydrazine, nitrogen, ammonia, and hydrogen can be described, respectively, as follows:

$$\nabla\cdot\left(\varepsilon_g\rho_g u_g Y_{g,N_2H_4} + D_{N_2H_4}\nabla Y_{g,N_2H_4}\right) = m_{g,L} - \left(R_{het}^{N_2H_4} + R_{hom}^{N_2H_4}\right)M_{N_2H_4} \tag{15}$$

$$\nabla\cdot\left(\varepsilon_g\rho_g u_g Y_{g,NH_3} + D_{NH_3}\nabla Y_{g,NH_3}\right) = \left(R_{het}^{N_2H_4} - R_{het}^{NH_3}\right)M_{NH_3} \tag{16}$$

$$\nabla\cdot\left(\varepsilon_g\rho_g u_g Y_{g,N_2} + D_{N_2}\nabla Y_{g,N_2}\right) = \frac{1}{2}\left(R_{het}^{N_2H_4} + R_{het}^{NH_3}\right)M_{N_2} \tag{17}$$

$$\nabla\cdot\left(\varepsilon_g\rho_g u_g Y_{g,H_2} + D_{H_2}\nabla Y_{g,H_2}\right) = \left(\frac{1}{2}R_{het}^{N_2H_4} + \frac{3}{2}R_{het}^{NH_3}\right)M_{H_2} \tag{18}$$

where $M_{N_2H_4}$, M_{NH_3}, M_{N_2}, and M_{H_2} are the molecular weights of hydrazine, ammonia, hydrogen, and nitrogen, respectively. $D_{N_2H_4}$, D_{NH_3}, D_{N_2}, and D_{H_2} are the effective mass-diffusion coefficients for hydrazine, ammonia, hydrogen, and nitrogen, respectively.

Mass exchange between the gas and the liquid

In the hydrazine monopropellant propulsion system, the liquid hydrazine is driven through the capillary tube by high-pressure nitrogen and atomized into small droplets via the atomizer at the exit of capillary tube. Then, the liquid droplets are jetted into the packed bed and contacted with the hot catalyst. In this process, when the mixture temperature is lower than the hydrazine boiling point, the vapor pressure on the surface of the droplet is equal to the saturated vapor pressure. Here, the gas-liquid mass exchange is mainly dominated by the gas-liquid mass transfer. With the chemical energy released by the catalytic decomposition of hydrazine, the mixture is heated to reach or exceed the hydrazine boiling point. In this case, when the droplet approaches the hot catalyst, the dynamics of the liquid droplet most likely occur in two cases: the liquid droplet spreads over the hot surface of the catalyst, and the liquid droplet is elastically repelled by the vapor cushion that forms beneath it on the hot catalyst surface. For the first case, the gas-liquid mass exchange is determined by the liquid-solid heat transfer. For the second case, the value can be described as the rate of liquid droplet burning in the high-temperature gas products or the gas-liquid heat transfer. Which case occurs in the liquid droplet strongly depends on the overheating extent of the catalyst and the droplets velocity and size and physical properties. If the catalyst overheating increases, the probability of the second case is higher. However, under the same catalyst surface temperature, the larger inertia of the liquid droplet would increase the probability of its spreading over the particle surface. In addition, the viscosity, heat capacity, and other physical properties are also important parameters for determining the action of the liquid droplet.

Based on the above analysis, when the temperature of the mixture is lower than the liquid hydrazine boiling point, the evaporation rate can be written as

$$m_{g,L} = k_{g,L}\frac{6}{d_p}M_{N_2H_4}(1-\varepsilon_g)\left(c_{N_2H_4}^{*} - c_{N_2H_4}^{b}\right) \tag{19}$$

where $k_{g,L}$ is the gas-liquid mass-transfer coefficient, d_p is the liquid droplet diameter, $c_{N_2H_4}^{*}$ is the concentration of hydrazine-saturated steam at the corresponding temperature, and $c_{N_2H_4}^{b}$ is the concentration of hydrazine in the gas mixture. According to Assumption 1, $k_{g,L}$ can be calculated as:

$$k_{g,L} = Sh\frac{D_{N_2H_4}}{d_p} = 2.0\frac{D_{N_2H_4}}{d_p} \tag{20}$$

When the mixture temperature exceeds the hydrazine boiling point, the evaporation rate can be written as

$$m_{g,L} = (1-\alpha)m_g + \alpha m_s \tag{21}$$

where m_g and m_s are the evaporation rates of the liquid droplet for the first case and the second case, respectively, and α is the collision probability between the liquid droplet and the hot catalyst surface. In the first case, the gas-liquid mass exchange can be evaluated by the liquid droplet burning model in a high-temperature gas in free space. Using the energy conservation theory,[37] m_g can be expressed as

$$m_g = 12\frac{(1-\varepsilon_g)\pi\lambda_m}{d_p{}^2 c_{p,m}}\ln\left(1 + \frac{c_{p,m}(T_m - T_b)}{h_{fg}}\right) \tag{22}$$

where T_b is the hydrazine boiling point, and h_{fg} is the liquid hydrazine latent heat of evaporation.

In the second case, according to Buyevich's theory,[38] m_s can be written as

$$m_s = \alpha_{s,L}(1-\varepsilon_b)\frac{6}{d_s}\frac{(T_s - T_b)}{h_{fg} + c_{p,m}(T_m - T_b)} \tag{23}$$

where $\alpha_{s,L}$ is the liquid-solid heat-transfer coefficient, which can be evaluated through the results reported by Ganic and Rohsenow.[39] In their article,[39] the evaporation effectiveness factor was defined to simplify the calculation for the liquid-solid heat transfer and can be written as

$$\eta_{vap} = \exp\left(1 - \left(\frac{T_s}{T_b}\right)^2\right) \tag{24}$$

Therefore, the liquid-solid heat transfer equation can be written as

$$q_{s,L} = u_m\varepsilon_L\rho_L h_{fg}\eta_{vap} \tag{25}$$

and the liquid-solid heat-transfer coefficient can be expressed as

$$\alpha_{s,L}=\frac{q_{s,L}}{T_s-T_b} \tag{26}$$

Regarding the calculation of the collision probability α, Buyevich et al.[38] first numerically analyzed the case of a single-obstacle particle with various shapes. Recently, Martynenko et al.[36] made improvement by studying spherical particles in a packed bed, and the numerical results were fitted to obtain the following equation:

$$\alpha=\left(\frac{(1-\varepsilon_b)6}{\pi}\right)^{1/3}\left(0.093+0.387Stk-0.054Stk^2\right) \tag{27}$$

where Stk is the Stokes dimensionless number, which can be expressed as

$$Stk=\frac{\rho_L d_p^2 u_m}{36\mu_m d_s} \tag{28}$$

In Kesten's model, the authors[23] assumed that the energy released by the reaction at the entrance of the packed bed was fully used to heat and vaporize the liquid hydrazine until the liquid was totally vaporized. When the mixture temperature is lower than the hydrazine boiling point, the gas-liquid mass exchange is assumed to be zero, and the hydrazine concentration in this region can be calculated from the saturated vapor pressure of liquid hydrazine at the corresponding temperature. When the mixture temperature reaches or exceeds the hydrazine boiling point, the reaction heat is entirely used to vaporize the liquid hydrazine. Therefore, the vaporization rate of the liquid can be written as

$$m_{g,L}=\frac{\left(R_{het}^{N_2H_4}+R_{hom}^{N_2H_4}\right)\Delta H_r^{N_2H_4}+R_{het}^{NH_3}\Delta H_r^{NH_3}}{h_{fg}} \tag{29}$$

Zhou et al.[30] developed a 1-D model to analyze the catalytic decomposition of H_2O_2 in a microthruster system. In his model, the system was first assumed to be divided into five independent regions: (I) the early heating of the monopropellant to the water boiling point; (II) the vaporization of liquid water; (III) the additionally heating the hydrogen peroxide to its boiling point; (IV) the vaporization of hydrogen peroxide; and (V) the gas-phase decomposition of hydrogen peroxide. However, to simplify the numerical calculation processes, regions I to IV was ignored in their model. Therefore, the inlet boundary could be set as the liquid vaporization products.

Gas-phase reaction rate

The kinetic expression of the homogeneous vapor-phase decomposition of hydrazine has been investigated by a number of researchers.[40,41] The acceptable Arrhenius equation can be written as

$$k_{hom}^{N_2H_4}=2.14\times10^{14}\exp\left(-\frac{1.523\times10^5}{RT_m}\right) \tag{30}$$

Similarly, the kinetic parameters for the catalytic decomposition of hydrazine can be found in the following equation in the references[41]:

$$k_{het}^{N_2H_4}=1.0\times10^{10}\exp\left(-\frac{1.15\times10^4}{RT_m}\right) \tag{31}$$

The kinetic expression for the vapor-phase catalytic decomposition of ammonia on platinum catalysts was reported by Melton et al.[42,43]:

$$k_{het}^{NH_3}=3.0\times10^{10}\exp\left(-\frac{2.31\times10^5}{RT_m}\right) \tag{32}$$

The gas-solid mass transfer should be considered because the catalytic reaction is so fast that, especially for hydrazine decomposition even at low temperatures, the reaction rate is mainly dominated by the mass transfer between the gas phase and the solid. Because the catalytic materials are impregnated on the interior and exterior surfaces of the porous particles, the diffusion of the reactants into the porous structure of the particles must also be considered. However, to simplify the numerical simulation process, the effect of thermal conduction inside the porous particles on the intraparticle diffusion effectiveness factor is neglected. Therefore, the following mass conversion equations can be expressed[44]:

$$R_{het}^{N_2H_4}=k_{N_2H_4}\eta_{N_2H_4}c_{N_2H_4}^s=k_{g,s}^{N_2H_4}\frac{6}{d_p}\left(c_{N_2H_4}^b-c_{N_2H_4}^s\right) \tag{33}$$

$$R_{het}^{NH_3}=k_{NH_3}\eta_{NH_3}\frac{c_{NH_3}^s}{\left(c_{H_2}^s\right)^{1.6}}=k_{g,s}^{NH_3}\frac{6}{d_p}\left(c_{NH_3}^b-c_{NH_3}^s\right) \tag{34}$$

$$R_{het}^{NH_3}=k_{NH_3}\eta_{NH_3}\frac{c_{NH_3}^s}{\left(c_{H_2}^s\right)^{1.6}}=k_{g,s}^{H_2}\frac{6}{d_p}\left(c_{H_2}^b-c_{H_2}^s\right) \tag{35}$$

Because the diffusion rate of hydrogen is larger than that of ammonia, Eqs. 34 and 35 can be expressed as:

$$R_{het}^{NH_3}=k_{NH_3}\eta_{NH_3}\frac{c_{NH_3}^s}{\left(c_{H_2}^b\right)^{1.6}}=k_{g,s}^{NH_3}\frac{6}{d_p}\left(c_{NH_3}^b-c_{NH_3}^s\right) \tag{36}$$

where $\eta_{N_2H_4}$ and η_{NH_3} are the intraparticle diffusion effectiveness factors for the hydrazine catalytic decomposition and the catalytic dissolution of ammonia, respectively. c_i^b and c_i^s are the concentration of hydrazine, ammonia, or hydrogen in the free gas phase and on the surface of the catalyst particles, respectively.

By solving the equations for the reaction coupled with the intraparticle diffusion[44] in the catalyst particles, an analytical expression for the effectiveness coefficient of the intraparticle diffusion can be obtained as

$$\eta_i=\frac{1}{\phi_i}\left[\frac{1}{th(3\phi_i)}-\frac{1}{3\phi_i}\right] \tag{37}$$

where ϕ_i is the Thiele modulus number for the catalytic decomposition reaction of hydrazine or ammonia, which can be calculated as:

$$\phi_i=\frac{d_c}{6}\sqrt{\frac{k_{het}^i}{D_i}} \tag{38}$$

Here, D_i^e is the effective diffusion coefficient for hydrazine, ammonia, and hydrogen in the catalyst pore, which can be evaluated by the formula $D_i^e=D_i\frac{\varepsilon_c}{\tau}$. τ is the tortuosity factor and assumed to be 2. The gas-solid mass-transfer coefficient for each pure component can be expressed as

$$k_{g,s}^i=2.0\varepsilon_b\frac{D_i}{d_c}+0.69\frac{D_i}{d_c}\left(\frac{U_m d_c\rho_g}{\varepsilon_b\mu_g}\right)^{1/2}\left(\frac{\mu_g}{\rho_g D_i}\right)^{1/3} \tag{39}$$

where the superscript and subscript i represent hydrazine, ammonia, and hydrogen.

Parameters

Thermal conductivity

Thermal Conductivity of the Gas Mixture. According to the Champan–Enskog kinetic theory of gases,[45] the thermal conductivity of a pure gas is a function proportional to the square root of the temperature. The thermal conductivity of a gas at a certain temperature can be expressed as

$$\lambda_{g,i}=\lambda^{*}_{g,i}\sqrt{\frac{T}{T^{*}}} \tag{40}$$

where $\lambda^{*}_{g,i}$ is the thermal conductivity of ith pure gas at the reference temperature T^{*}, which is given in the Supporting Information. The thermal conductivity of the gas mixture is computed based on a simple mole fraction average of the pure specie's conductivities:

$$\lambda_g=\sum_i \lambda_{g,i}x_i \tag{41}$$

For correctly predicting the mass and heat transfer in the packed bed, we considered the influence of dispersion on the heat transfer. In this study, because the porous structure in the packed bed is assumed to be isotropic, the heat-transfer coefficient due to both the transverse and longitudinal dispersion of the mixture can be calculated as[46]

$$\lambda_d=\lambda_g\rho_m c_{p,m}\frac{Pe}{2} \tag{42}$$

where $Pe=\frac{u_m d_c}{\lambda_g}$ is the dimensionless Peclet number. Therefore, the effective thermal conductivity of the mixture can be written as

$$\lambda_m=\lambda_g+\lambda_d \tag{43}$$

Effective Thermal Conductivity of the Porous Catalyst. The thermal conductivity of the homogeneous solid mixture can be as simple as a sum of the pure solid thermal conductivity multiplied by the component mass fraction, so the expression can be written as:

$$\lambda_{s,m}=\sum_i \lambda_{s,i}y_i \quad (i=Al_2O_3, Ir) \tag{44}$$

where $\lambda_{s,i}$ is thermal conductivity of the ith component of the pure solid, which is assumed to be constant in this study and given in the Supporting Information, $\lambda_{s,m}$ is the thermal conductivity of the solid mixture. Because the catalyst is a porous media, its effective thermal conductivity can be obtained by the following equation[47]:

$$\frac{\lambda_s}{\lambda_{s,m}}=\frac{1+2\gamma\varepsilon_c+(2\gamma^3-0.1\gamma)\varepsilon_c{}^3+0.05\varepsilon_c{}^3\exp(4.5\gamma)}{1-\gamma\varepsilon_c} \tag{45}$$

Here, ε_c is the porosity of the catalyst. The parameter γ can be expressed as

$$\gamma=\frac{\lambda_g/\lambda_s-1}{\lambda_g/\lambda_s+2} \tag{46}$$

Effective Thermal Conductivity of the Packed Bed. The effective thermal conductivity of the packed bed saturated with a stagnant fluid consists of four distinct heat transfer mechanisms: (1) heat transfer through the contact surface of the solid particles; (2) conduction through the stagnant fluid near the contact surface; (3) radiation between the solid surfaces (when the radiation of the gas in the void is neglected); and (4) conduction through the solid phase. Kunii and Smith[48] considered these mechanisms and developed a correlation to estimate the effective thermal conductivity of the solid structure in packed beds, which can be given as

$$\frac{k^{e}_s}{k_g}=\varepsilon_b\left(1+\frac{\beta k_{rv}d_c}{k_g}\right)+\frac{\beta(1-\varepsilon_b)}{\left(\frac{1}{1/\psi_t+k_{rs}d_c/k_g}+\frac{\xi}{\kappa}\right)} \tag{47}$$

where κ can be calculated by the formula $\kappa=\frac{k_s}{k_g}$. k_{rs} and k_{rv} are the radiation from solid to solid and void to void, respectively, which can be calculated as

$$k_{rs}=4\sigma T^3\frac{\varepsilon_r}{2-\varepsilon_r} \tag{48}$$

$$k_{rv}=\frac{4\sigma T^3}{1+\frac{\varepsilon_b}{2(1-\varepsilon_b)}\frac{(1-\varepsilon_r)}{\varepsilon_r}} \tag{49}$$

where σ is the Stefan–Boltzmann constant, and the empirical value β is $\beta=0.895$ for a close packing of spheres and $\beta=1$ for a loosely packed bed. The empirical value ξ was chosen to be $2/3$. The empirical constant ψ_t, which is defined as the coordination flux number, is a function of the number of contacts responsible for heat transfer. For basic loose packing Kunii and Smith[48] argued that $n=1.5$ and for a close packing $n=4\sqrt{3}$. When the value of ε_b is greater than 0.260 and smaller than 0.476, ψ_t can be approximated by

$$\psi_t=\psi_2+(\psi_1+\psi_2)\frac{\varepsilon_b-0.260}{0.216} \tag{50}$$

where ψ_1 and ψ_2 are evaluated for a loose and close arrangement, which can be obtained from

$$\psi_{1,2}=\frac{0.5\left(\frac{\kappa-1}{\kappa}\right)^2\sin^2\theta_0}{\ln(\kappa-(\kappa-1)\cos\theta_0)-\left(\frac{\kappa-1}{\kappa}\right)(1-\cos\theta_0)}-\frac{2}{3\kappa} \tag{51}$$

Here, θ_0 is the fraction of the total heat-transfer coefficient associated with one contact point between two spheres, which can be obtained by:

$$\sin^2\theta_0=1/n \tag{52}$$

Gas diffusion coefficient

The mass diffusivity coefficient D_{AB} for most binary gas mixtures can be obtained from handbooks. The value of hydrazine is predicted within approximately 5% by Chapman–Enskog kinetic theory, which can be written as

$$D_{AB}=0.0018583\sqrt{T^3\left(\frac{1}{M_A}+\frac{1}{M_B}\right)}\frac{1}{p\sigma^2_{AB}\Omega_{AB}} \tag{53}$$

where M_A and M_B are the molecular weights for substances A and B, respectively. The dimensionless quantity Ω_{AB} is the "collisional integral" for diffusion and is a function of dimensionless temperature kT/ε_{AB}. With the prediction of kT/ε_{AB}, the value of Ω_{AB} can be obtained from references.[45] Therefore, k/ε_{AB} and σ_{AB} can be calculated as:

$$\frac{\varepsilon_{AB}}{k}=\sqrt{\frac{\varepsilon_A}{k}\frac{\varepsilon_B}{k}} \tag{54}$$

$$\sigma_{AB}=\frac{1}{2}(\sigma_A+\sigma_B) \tag{55}$$

Here, σ_A is the molecule characteristic diameter of molecules, often called the collision diameter, and ε_A is the

characteristic energy or the maximum energy of attraction between a pair of molecules. σ_A and ε_A for most substances are available in literature, but the properties of the gas-phase hydrazine considered in this study are not reported. Therefore, the following equations are usually used to estimate properties for unknown substances from the properties of the fluid at the critical point, which can be expressed as

$$\frac{\varepsilon_A}{k}=0.77T_c^A \tag{56}$$

$$\frac{\varepsilon_A}{k}=2.44\left(\frac{T_c^A}{P_c^A}\right)^{1/3} \tag{57}$$

where T_c^A and P_c^A are the relevant critical temperature and critical pressure, respectively.

D_i used in solving Eqs. 15 to 18, is the mass diffusion coefficient for species i in mixtures, and it can be computed as

$$D_i=\frac{1-x_i}{\sum_{j,j\neq i}\left(x_j/D_{ij}\right)} \tag{58}$$

where x_i is the mole fraction of componenti.

Heat capacity

The heat capacity of a pure component is computed as a function of temperature. The heat capacity of a mixture is evaluated by the mass-weighted mixing law of pure-species heat capacities, which can be written as

$$c_{p,m}=\sum_i c_{p,i}y_i \quad \ldots\ldots (i=N_2H_4, NH_3, H_2, N_2) \tag{59}$$

where y_i is the mass fraction of pure species i. The relevant pure species heat capacities are given in the Supporting Information.

Numerical solution method and boundary condition

In this article, the governing equations are solved by the mixture model in the commercial Fluent 6.3.26 package and the corresponding UDS, UDF, and UDM functions. Gambit 2.2 is used to generate the computational grid. The momentum, mass, and energy conservation equations are discretized by the second-order upwind differencing scheme over the finite volume used. The coupled algorithm under the pressure-based solver is used for the momentum and continuity equations.

The inlet boundary is designed as a mass flow, where the temperature is 300 K. The outlet boundary is a pressure boundary. Other boundary conditions are specified as walls. The influence of wall on the fluid flow is neglected, and the heat flux at the walls is specified as a constant zero.

The sketch of the thruster is shown in Figure 1. Theoretically, only liquid is present at the boundary of the entrance. In fact, because the pressure decreases abruptly at the exit of capillary tube, it is inevitable that the liquid is partially vaporized. Therefore, in our solution process, 1 wt % of the liquid is assumed to be vaporized to gas at the inlet boundary, and it has been proven that this setting can also improve the stability of the solution.

In this solution, the under-relaxation factors are set to 0.8 for the density, 0.9 for the energy, and 0.75 for the species transport equations. The Courant number is set to 2.0, and the explicit relaxation factors for momentum and pressure are defined to be 0.75. The convergences criteria of the sum

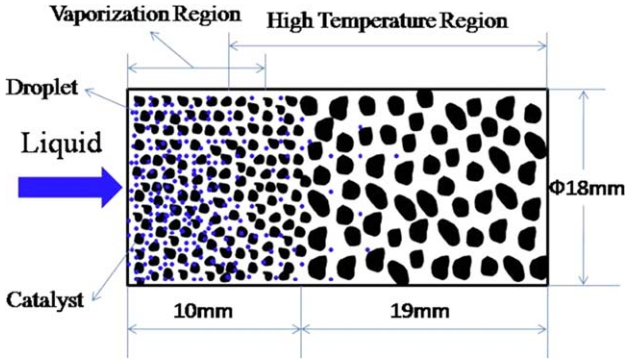

Figure 1. Sketch of the physical model.

[Color figure can be viewed in the online issue, which is available at wileyonlinelibrary.com.]

of the normalized absolute residuals, which are defined as the sum of the absolute residuals values per grid point over all of the grid points normalized by the value of that same summation at the beginning of the iterative solution procedure, are set to 1.0×10^{-6} for continuity equation, 1.0×10^{-9} for the energy equation and 1.0×10^{-5} for the rest of equations. This solution process is performed on a computer server with 24 CPU (3.0 GHz) and 128 GB memory.

Results

To decouple the effect of calculating the mesh grid, the mesh was checked before all of the simulations. Our results shown that the effect of calculating mesh grid can be neglected for all calculations when the mesh size is 0.025×0.05 mm.

Influence of mass flux

To validate this model, experiments for liquid hydrazine decomposition in a packed bed were implemented in a vacuum chamber with a pressure of 0.5 Pa, and a detailed description of the experimental equipment can be found in the Supporting Information. A packed bed with an ID of 18 mm and a length of 29 mm was used and filled with the catalyst particles with a diameter of 0.8 mm. In the experimental process, the liquid hydrazine was compressed into the packed bed through the capillary tubes by high-pressure nitrogen, and the desired mass flux was obtained by adjusting the nitrogen pressure. Quartz wool with a thickness of 20 mm was used as an insulating layer around the packed bed to prevent the heat loss from the packed bed surface, which was further covered by aluminum tissue to decrease the heat radiation between the packed bed and the wall of the vacuum chamber. Therefore, the temperature in the packed bed can be approximately described by the surface temperature, which was determined by seven K-type thermocouples fixed on the surface of the packed bed at the intervals of 5 mm. In this experiment, the mass flow of hydrazine was set to 5.5 kg m^{-2} s^{-1}, the inlet pressure was 0.7 MPa, and the reaction pressure in the packed bed was 0.6 MPa. The variation of the reaction pressure with time is given in the Supporting Information. In addition, the packed bed was heated to the desired temperature before feeding the liquid hydrazine to avoid damaging the catalyst in the low-temperature start-up. The relevant experimental data are shown in Figure 2, and to reach steady state, all of the experiments here were carried out for more than 200 s.

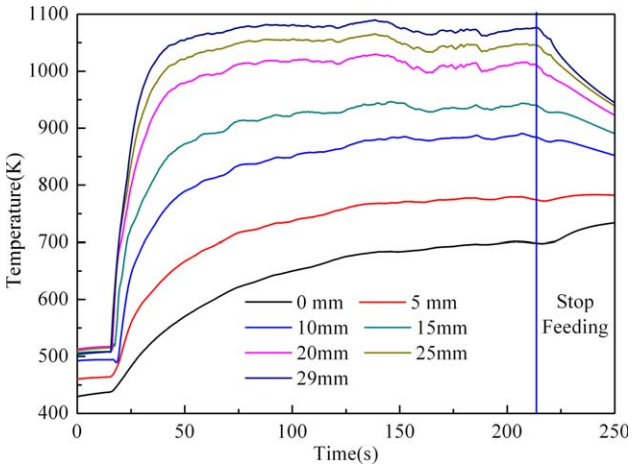

Figure 2. Variation of temperature with time at the different axial positions of the packed bed.

[Color figure can be viewed in the online issue, which is available at wileyonlinelibrary.com.]

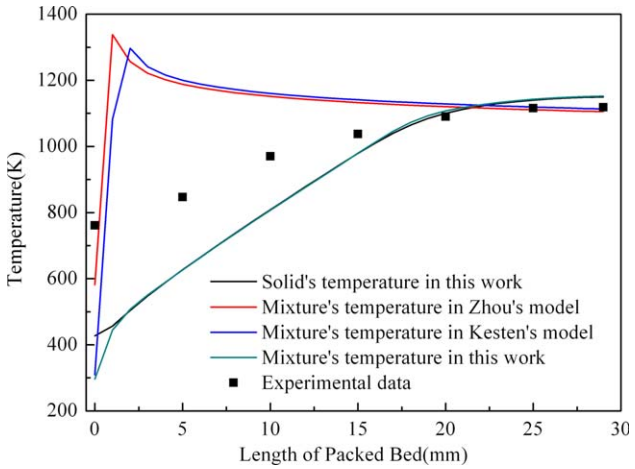

Figure 4. Comparison of the temperature distribution between the simulation results and the experimental data (Mass flow: 9.44 kg m^{-2} s^{-1}, Chamber pressure: 1.05 MPa).

[Color figure can be viewed in the online issue, which is available at wileyonlinelibrary.com.]

When the liquid hydrazine stopped feeding, the temperatures in the back region of the packed bed began to decrease, but the temperature near the entrance of the packed bed increased due to the disappearance of cooling from the latent heat of liquid hydrazine vaporization, as described in Figure 2. This observation also indicates that considering the effect of liquid vaporization is necessary in simulating the liquid hydrazine decomposition process in the packed bed.

Comparisons between the experimental results and three model predictions of the axial distribution of the mean temperature with various liquid hydrazine mass fluxes are shown in Figures 3–5. As the plots in these figures show, the simulation results based on the model developed in this article have better agreements with the experimental data than the results of other models. According to the predictions from Zhou's and Kesten's models, the high-temperature region appears in the front of the packed bed, which strongly disagrees with the experimental results. The possible reason for this disagreement is the deviation of the real rate of liquid hydrazine evaporation from their assumptions. In their models, the limitations of the transport phenomena for the liquid vaporization are ignored; all of energy released by the hydrazine decomposition reaction is used to vaporize the liquid hydrazine, which would result in the liquid hydrazine being rapidly vaporized and then catalytically decomposed near the entrance of the packed bed. As a result, the system temperature quickly increases and reaches a maximum in this region. In fact, due to the limitation of transport phenomena between phases, the chemical energy released by the hydrazine catalytic decomposition is only partially used to vaporize the liquid hydrazine, so the real rate of liquid hydrazine vaporization in the packed bed should be smaller than of the rate predicted in Kesten's model. As the experimental data show in Figures 2–5, the high-temperature region realistically appears in the back of the packed bed, which agrees

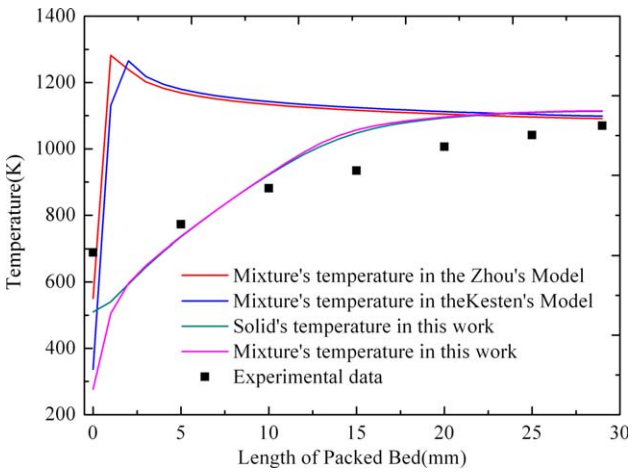

Figure 3. Comparison of the temperature distribution between the simulation results and the experimental data (Mass flow: 5.5 kg m^{-2} s^{-1}, Chamber pressure: 0.6 MPa).

[Color figure can be viewed in the online issue, which is available at wileyonlinelibrary.com.]

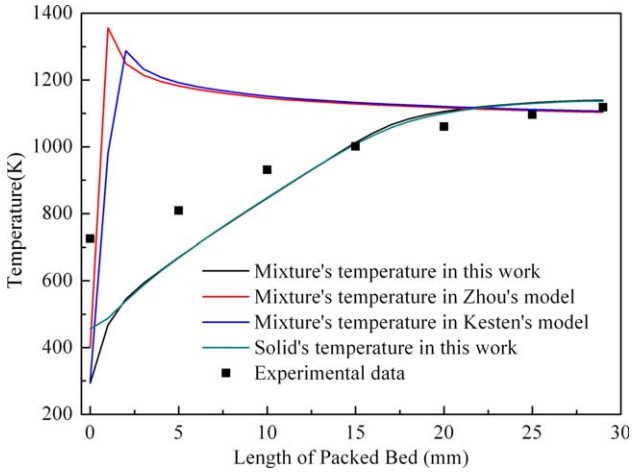

Figure 5. Comparison of the temperature distribution between the simulation results and the experimental data (Mass flow: 11.79 kg m^{-2} s^{-1}, Chamber pressure: 1.4 MPa).

[Color figure can be viewed in the online issue, which is available at wileyonlinelibrary.com.]

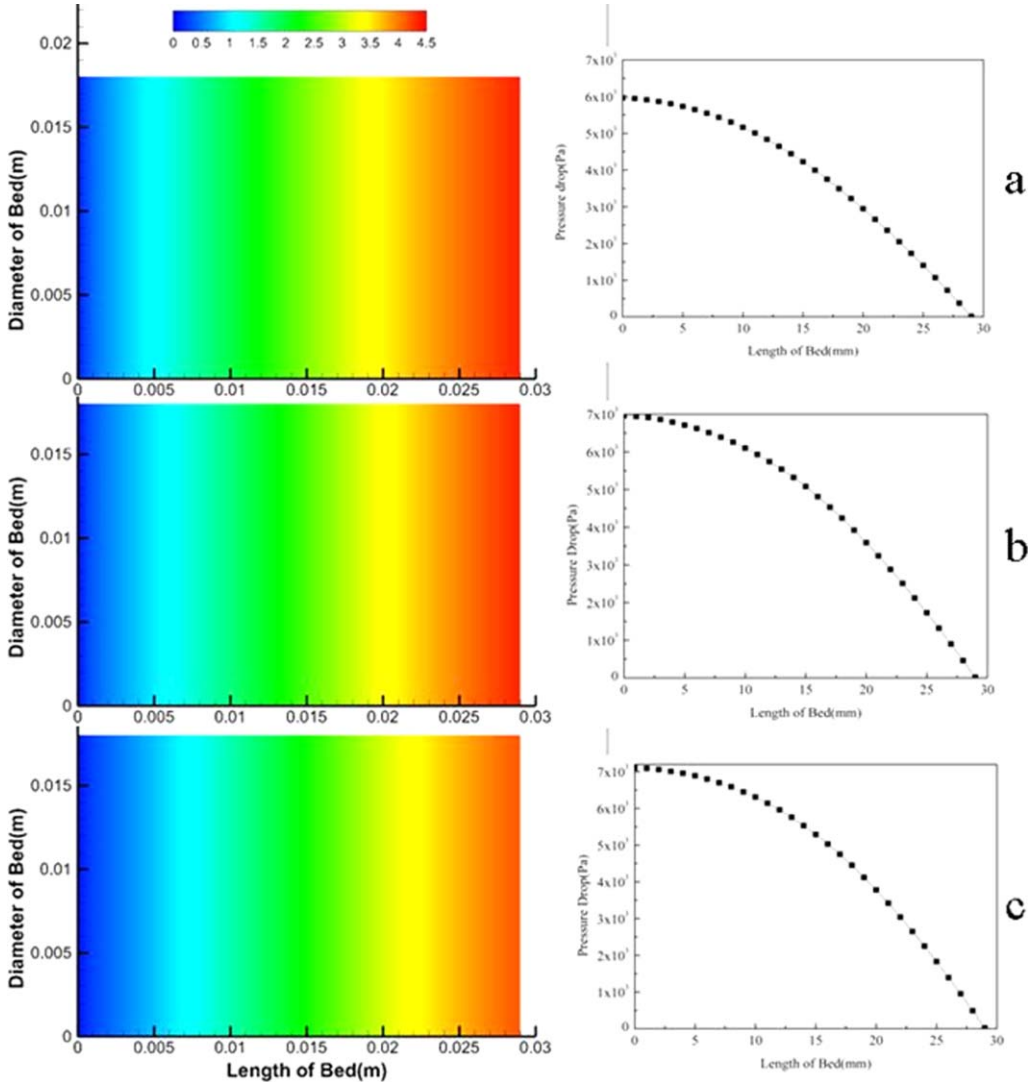

Figure 6. Distributions of the mixture velocity and the pressure drop for the different operational cases (a: Mass flux = 5.5 kg m^{-2} s^{-1}, Chamber pressure = 0.6 MPa; b: Mass flux = 9.44 kg m^{-2} s^{-1}, Chamber pressure = 1.05 MPa; c: Mass flux = 11.79 kg m^{-2} s^{-1}, Chamber pressure = 1.4 Mpa.

[Color figure can be viewed in the online issue, which is available at wileyonlinelibrary.com.]

with our model's prediction. This phenomenon is proven again by the video snapshot of the liquid hydrazine decomposed in the 2-D transparent quartz packed bed, given in the Supporting Information. For the model developed in this article, the deviation from the experimental results in the entrance as shown in Figures 3–5 is associated with the high thermal conductivity of the stainless steel shell of the packed bed, which makes the surface of the stainless steel shell near the entrance of packed bed heated by the high temperature region in the back of the packed bed. Therefore, the real temperature in this region should be lower than the experimental results and closer to our prediction. Based on our model's results, shown in Figures 3–5, the solid catalyst temperature is higher than that of the gas mixture near the entrance, which results from the solid catalyst near the entrance of the packed bed being heated by the high-temperature particles in the back of the packed bed. However, in the back of the packed bed, the relative temperature difference between the gas mixture and the solid disappears due to the improvement of the gas-solid heat transfer rate with increasing fluid velocity. Generally, improving the solid catalyst temperature near the entrance favors promoting the liquid droplet vaporization and stabilizing the performance of liquid hydrazine decomposition. Therefore, optimizing the energy balance over the whole packed bed through the relevant theoretical analysis is important for obtaining a good thruster system performance. In addition, both the experimental data and the simulation results in Figures 3–5 show that the high-temperature region moves forward to the back of the packed bed with an increasing mass flux of liquid hydrazine because more liquid is required to be vaporized. Based on the above analysis, it can be concluded that the performances of the packed bed in the entrance is mainly dominated by the liquid vaporization or the gas-liquid and liquid-solid heat transfer.

Figure 6 shows the distributions of the mixture's velocity and pressure drop under the different operational conditions. A comparison of parts a–c of Figure 6 indicates that although the mass fluxes of liquid hydrazine are increased from 5.5 to 11.79 kg m^{-2} s^{-1}, the velocity of the mixture at the outlet is not obviously improved because of the increase of mixture density as the reaction chamber pressure

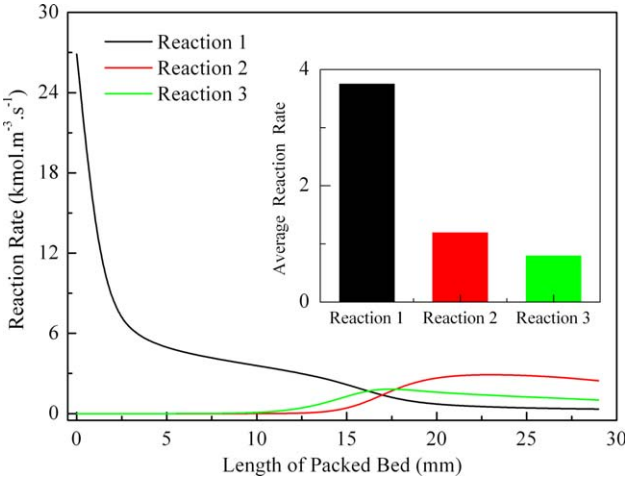

Figure 7. Axial distribution of the reaction rate for mass flux = 9.44 kg m^{-2} s^{-1} and chamber pressure = 1.05 MPa (Reaction 1: heterogeneous decomposition of hydrazine; Reaction 2: heterogeneous decomposition of ammonia; Reaction 3: homogeneous decomposition of hydrazine).

[Color figure can be viewed in the online issue, which is available at wileyonlinelibrary.com.]

increases. As shown in the right of Figure 6, the change of the pressure drop with increasing mass flux in our study can be ignored compared with the corresponding reaction chamber pressure.

According to the literature,[23] three main reactions occur in the packed bed. The axial distributions of every reaction rate under a certain condition are given in Figure 7. The heterogeneous decomposition reaction of hydrazine first occurs and reaches a maximum near the entrance of the packed bed. When the reaction system is heated by the chemical energy released by the heterogeneous reaction of hydrazine, due to the intraparticle diffusion effect of the reactants along with the hydrazine depletion in the back region of the packed bed, the homogeneous decomposition of hydrazine begins, and its reaction rate exceeds that of the relevant heterogeneous reaction. According to the bar chart for the mean reaction rate over the whole packed bed shown in Figure 7, the hydrazine catalytic decomposition reaction, which is three times faster than the homogeneous decomposition reaction of hydrazine and ammonia, dominates the decomposition process of liquid hydrazine.

The axial distributions of the liquid voidage for various mass fluxes, shown in Figure 8, indicate that the liquid hydrazine is rapidly vaporized near the entrance due to the pressure abruptly changing and contacting the high-temperature catalyst. Additionally, the simulation results suggest that the length of the gas-liquid coexistence region is increased with improving mass flux. This length has been verified to be critical parameter for stabilizing the liquid hydrazine decomposition process in the packed bed.[49] According to the conclusions of a previous study, if the length of the gas-liquid coexistence region exceeds one-fifth of the length of the packed bed, the stability performance of the packed bed decreases.

In Figure 9, the axial distributions of the ammonia, hydrogen, and hydrazine molar fractions are presented for mass flux of 5.5 kg m^{-2} s^{-1} (black line), 9.44 kg m^{-2} s^{-1} (red line), and 11.79 kg m^{-2} s^{-1} (blue line). It can be seen that the hydrazine rapidly decomposes near the entrance, and the hydrogen and ammonia concentrations reach particular values. Then, the ammonia begins to be heterogeneously decomposed in the high-temperature region at the back of packed bed. The effect of the mass flux on the hydrazine decomposition reaction can be ignored, and the dissolution ratio of ammonia is slightly decreased when the mass flux increases.

Influence of the packing structure

In designing the packed bed for the catalytic decomposition of the liquid propellant, the catalyst size, and the relevant packing structure are often changed to optimize the

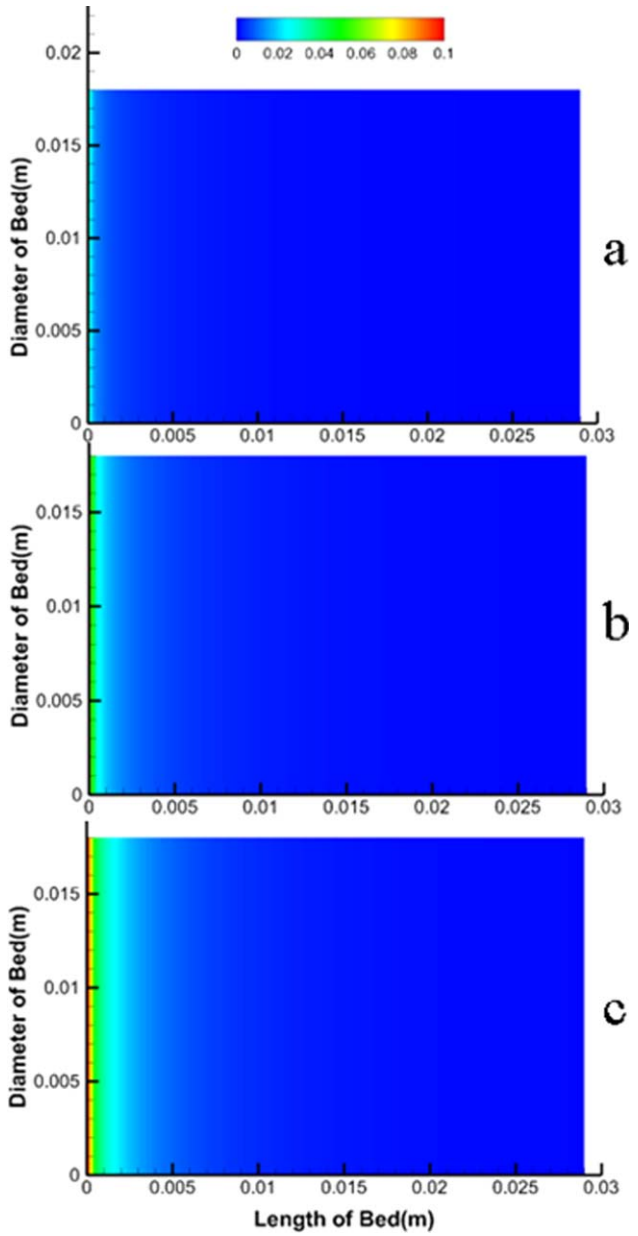

Figure 8. Axial distribution of the liquid volume fraction (a: Mass flux = 5.5 kg m^{-2} s^{-1}; b: Mass flux = 9.44 kg m^{-2} s^{-1}; Mass flux = 11.79 kg m^{-2} s^{-1}).

[Color figure can be viewed in the online issue, which is available at wileyonlinelibrary.com.]

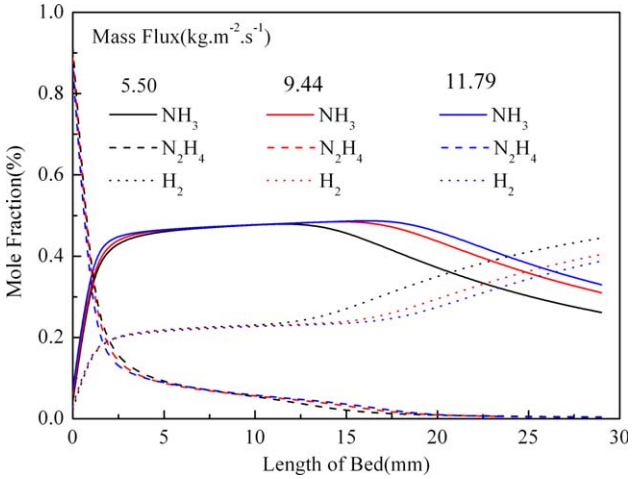

Figure 9. Axial distribution of the ammonia, hydrogen and hydrazine's mole fractions for the different mass fluxes.

[Color figure can be viewed in the online issue, which is available at wileyonlinelibrary.com.]

performance of packed bed. Due to the heterogeneous hydrazine decomposition reaction mainly dominated by the intraparticle diffusion of reactants, decreasing the particle size can improve the catalytic decomposition reaction rate of hydrazine but also can lead to a large pressure drop under the same fluid velocity. In this section, two types of particles, with diameters of 0.8×10^{-3} m and 1.4×10^{-3} m, were used, and five types of different packing structures were used. In Case 1, only the catalyst particles with diameters of 0.8×10^{-3} m were used. In Case 2, the particles with diameters of 0.8×10^{-3} m were packed in the region of length shorter than 1.5×10^{-2} m, and the rest of the packed bed was filled with the catalyst particles with diameters of 1.4×10^{-3} m. In Case 3, the region of length shorter than 10×10^{-2} m was filled with particles with diameters of 0.8×10^{-3} m, and the rest was filled with particles with diameters of 1.4×10^{-3} m. In Case 4, the region of length shorter than 5×10^{-3} m was filled with particles with diameters of 0.8×10^{-3} m, and the rest was filled with particles with diameters of 1.4×10^{-3} m. Finally, in Case 5, only particles with diameters of 1.4×10^{-3} m were used. The mass flux was set to be 9.44 kg m^{-2} s^{-1} and the reaction chamber pressure was 1.05 MPa.

The length of the packed bed filled by particles with ID 0.8×10^{-3} m in the entrance was decreased from 29 mm in Case 1 to 5 mm in Case 4. In Case 5, the particles with ID 1.4×10^{-3} m were used to pack the whole packed bed. The effect of the packing structure on the mixture velocity is shown in Figure 10. From this figure, it can be seen that the

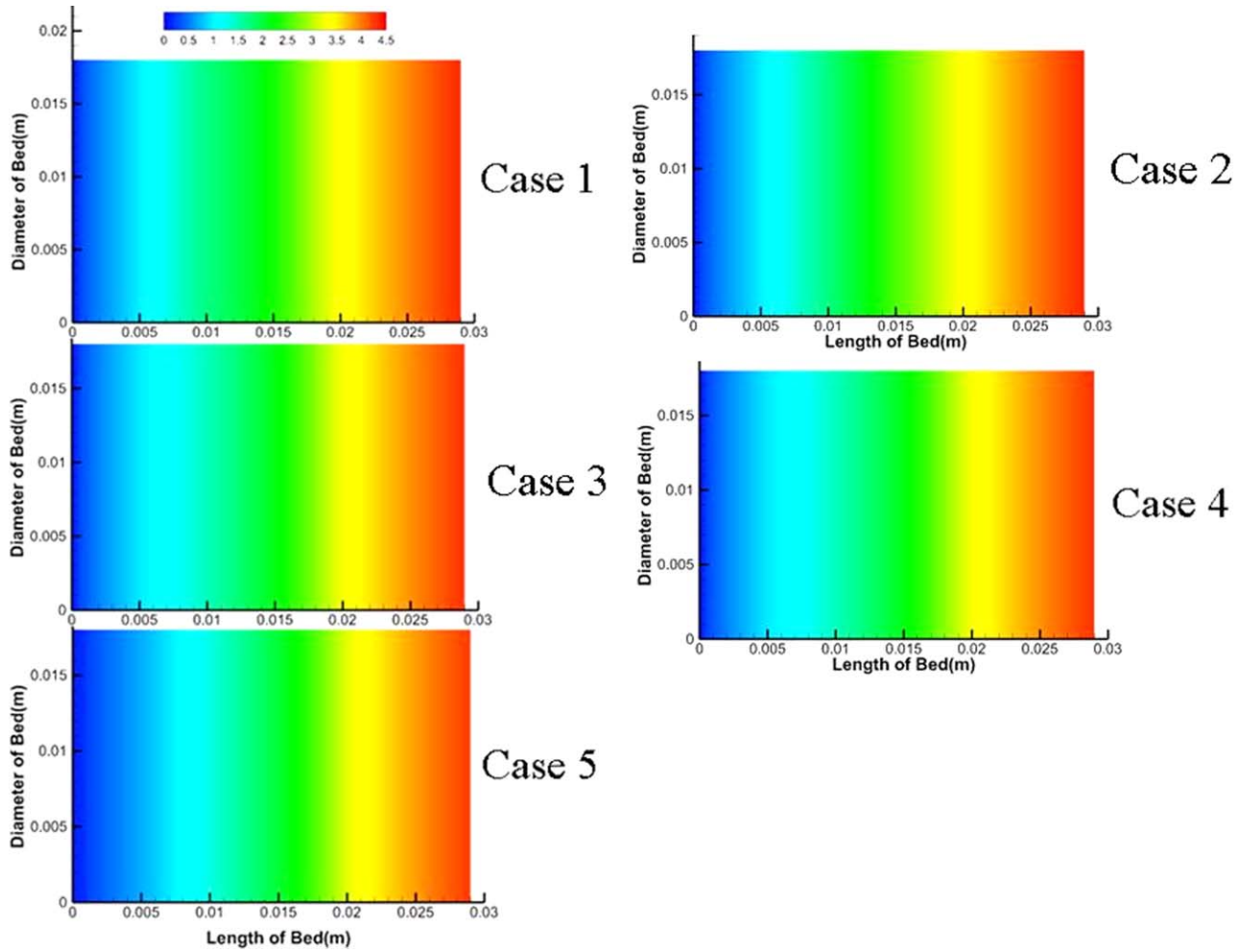

Figure 10. Distribution of the mixture velocity with various packing structures.

[Color figure can be viewed in the online issue, which is available at wileyonlinelibrary.com.]

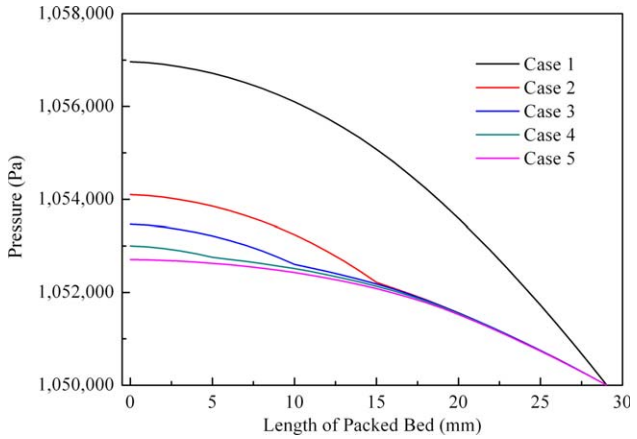

Figure 11. Axial distribution of the pressure with various packing structures.

[Color figure can be viewed in the online issue, which is available at wileyonlinelibrary.com.]

distributions of mixture velocity in Case 1 to Case 4 are nearly consistent and obviously different between Case 4 and Case 5. Therefore, the diameter of catalyst used and the relative packed length near the entrance of the packed bed are critical parameters for the axial distribution of the mixture velocity. The effect of packing structure on the mixture velocity is relative small and can be ignored only if the same particles are used in the entrance with the length bigger than 5 mm.

In optimizing the packed bed, the desired goal is to make the pressure drop as low as possible under the same thruster force. The effects of packing structures on the pressure drop based on our model's results are shown in Figure 11. From comparing the relevant calculated results for Case 1 to Case 5, it can be seen clearly that the difference of the pressure distributions among Cases 2, 3, 4, and 5 is small and can be almost ignored, but the pressure drop is obviously higher in Case 1. Based on Eq. 5, the pressure drop not only is determined by the fluid velocity but also strongly depends on the particle size. Because the fluid velocity near the entrance of packed bed is apparently lower than that in the back region

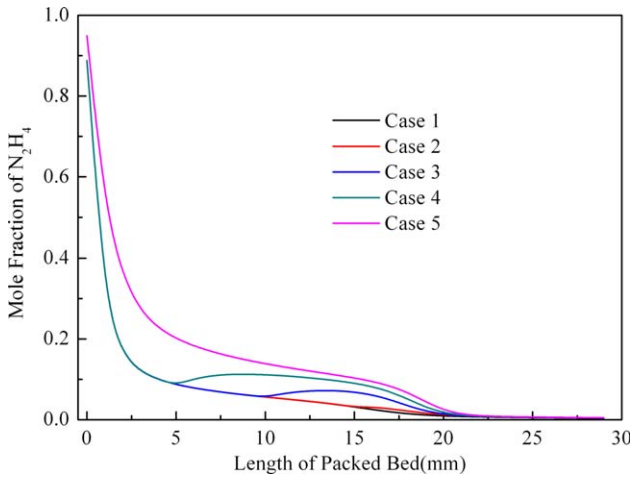

Figure 12. Axial distribution of the N_2H_4 mole fraction with various packing structure.

[Color figure can be viewed in the online issue, which is available at wileyonlinelibrary.com.]

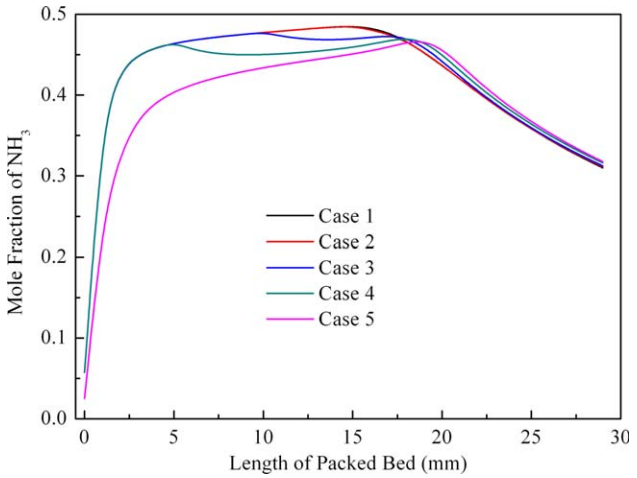

Figure 13. Axial distribution of the NH_3 mole fraction with various packing structures.

[Color figure can be viewed in the online issue, which is available at wileyonlinelibrary.com.]

of the packed bed, decreasing the particle size in this region does not lead to an obvious increase of packed bed pressure drop in Case 2 through Case 5. When the small particles are used in the region of high fluid velocity in the back of packed bed, the pressure drop is obviously increased as represented by Case 1.

The axial distributions of the N_2H_4 and NH_3 mole fractions for various packing structures are given in Figures 12 and 13, respectively, based on our model's results. Due to the catalytic and thermal decomposition, hydrazine is gradually converted into ammonia, nitrogen, and hydrogen from the entrance to the back of packed bed. In Case 1 and Case 2, although different sized catalysts are used in the region with the length bigger than 15 mm, the variation of the hydrazine mole concentration can be ignored. In Case 3 and Case 4, due to decreasing the length of the packed bed using small-particle size catalysts, the concentration of hydrazine in Case 4 is higher than that in Case 3, which can be explained by the reaction of hydrazine catalytic decomposition reaction mainly dominated by the gas intraparticle diffusion. Figure 13 gives the axial distributions of the NH_3 concentration in Case 1 to Case 5. With the decomposition of hydrazine, the NH_3 concentration is gradually increased from the entrance to the back of the packed bed. When the gas mixture has access to the high temperature in the back of the packed bed, the ammonia is further catalytically decomposed into hydrogen and nitrogen. In addition, because the ammonia decomposition reaction is mainly dominated by the intrinsic chemical reaction kinetics, the ammonia concentration at the outlet is almost constant in all cases.

In Figure 14, the distributions of the liquid volume fraction with various packing structures are given. The effects of the packing structure in Case 1 to Case 4 are small and can be ignored. In Case 5, the length of the gas-liquid coexistence region is obviously bigger than that in the other cases. The critical factor for determining the length of the gas-liquid coexistence region is the rate of liquid vaporization, which is mainly dominated by the gas-liquid and liquid-solid heat transfer. From Figure 14, it can be observed that the liquid is almost fully vaporized in the region of the packed bed shorter than 5 mm. In this region, the main thermal energy originates from the heterogeneous catalytic decomposition of

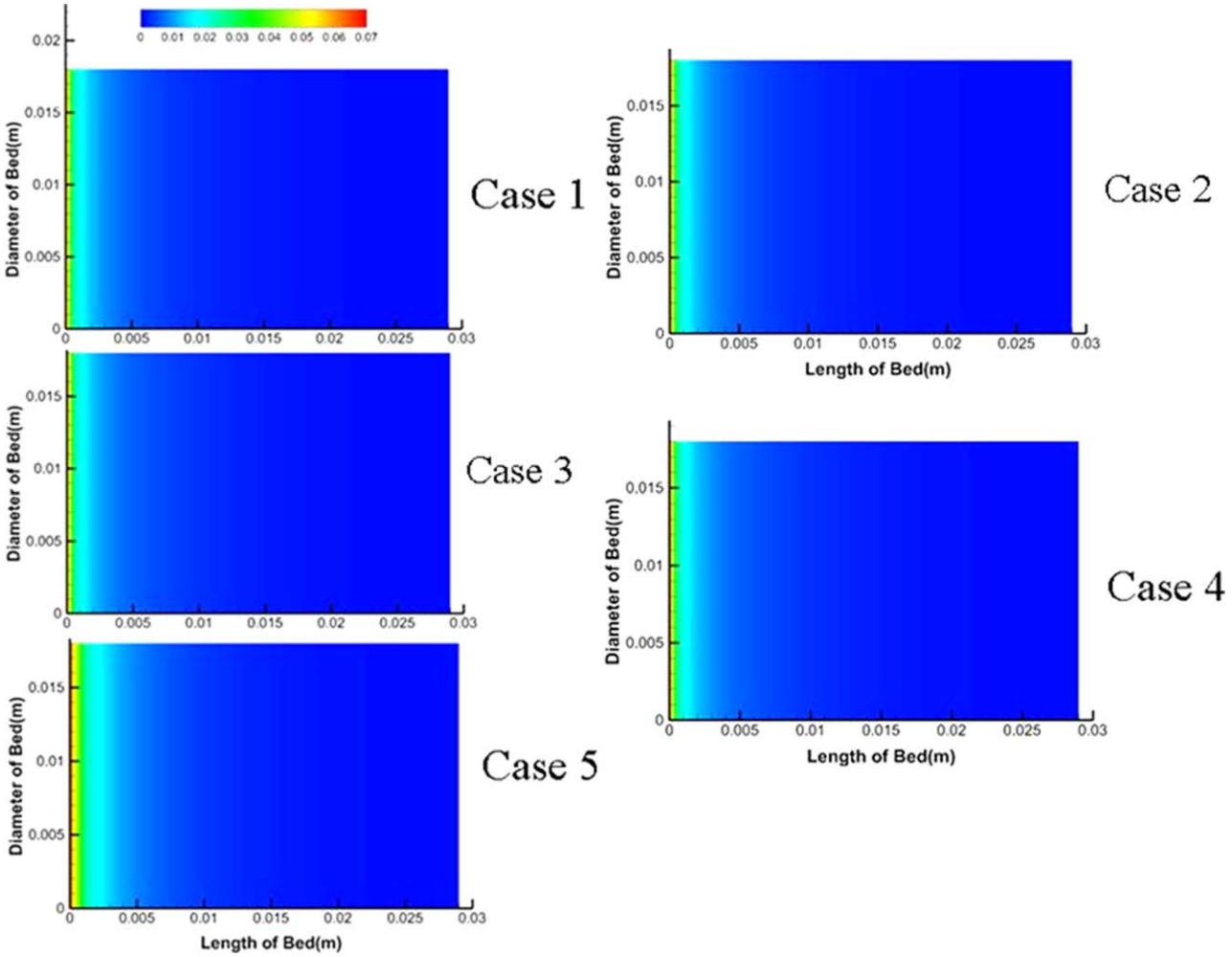

Figure 14. Distributions of the liquid volume fraction with various packing structures.

[Color figure can be viewed in the online issue, which is available at wileyonlinelibrary.com.]

hydrazine, which is dominated by the gas intraparticle diffusion, so using the small-particle size catalyst can improve the reaction rate and shorten the length of gas-liquid coexistence region. Based on the experimental data in the literature,[49] decreasing the length of the gas-liquid coexistence region favors stabilizing the whole thruster system, so the particle size in this region should be as possible as small in designing the packed bed.

The distribution of the gas mixture temperature is calculated by summing the released energy of hydrazine decomposition and the adsorbed energy of ammonia decomposition. Due to the ammonia decomposition reaction being dominated by the chemical kinetics, the influence of the packing structure on the reaction rate can be ignored. Therefore, the effect of the packing structure on the distribution of the mixture temperature is mainly determined by the hydrazine decomposition reaction. As shown in Figure 15, the distribution of the mixture temperature is almost consistent when the same particle size catalyst is used in packed bed with a length shorter than 15 mm, such as in Case 1 and Case 2, because the hydrazine has been fully converted in this region. However, with decreasing the length of using small particle sizes in Case 3 to Case 5, the high temperature region gradually moves forward to the outlet of the packed bed. Especially in Case 5, the change of the catalyst particle size near the entrance leads to the obvious difference for the temperature distribution in this region.

Discussion

The decomposition of liquid hydrazine in a packed bed is theoretically analyzed in detail and experimentally investigated here. In this system, the liquid hydrazine is first compressed into atomizers through capillary tubes by high pressure-nitrogen and then atomized into liquid droplets as described in Figure 1. Regarding the liquid droplet, two cases possibly occur, when the particle is jetted into the packed bed and contacted with the hot catalyst. If the overheating extent of the hot catalysts is small enough, due to the inertial force, the droplet can spread over, and make an actual touching with the surface of catalyst, and then be vaporized. In this case, the rate of liquid vaporization can be calculated by the liquid–solid heat transfer given in Eq. 22. However, in the second case, when the catalysts overheating exceeds the critical value, a thin intervening vapor layer between the droplet and catalyst would be formed through the intensive evaporation of the liquid droplet by the overheating catalyst radiation. It is possible that the droplet rebounds from the surface of the particle by excessive pressure. In this case, the rate of liquid evaporation, which is

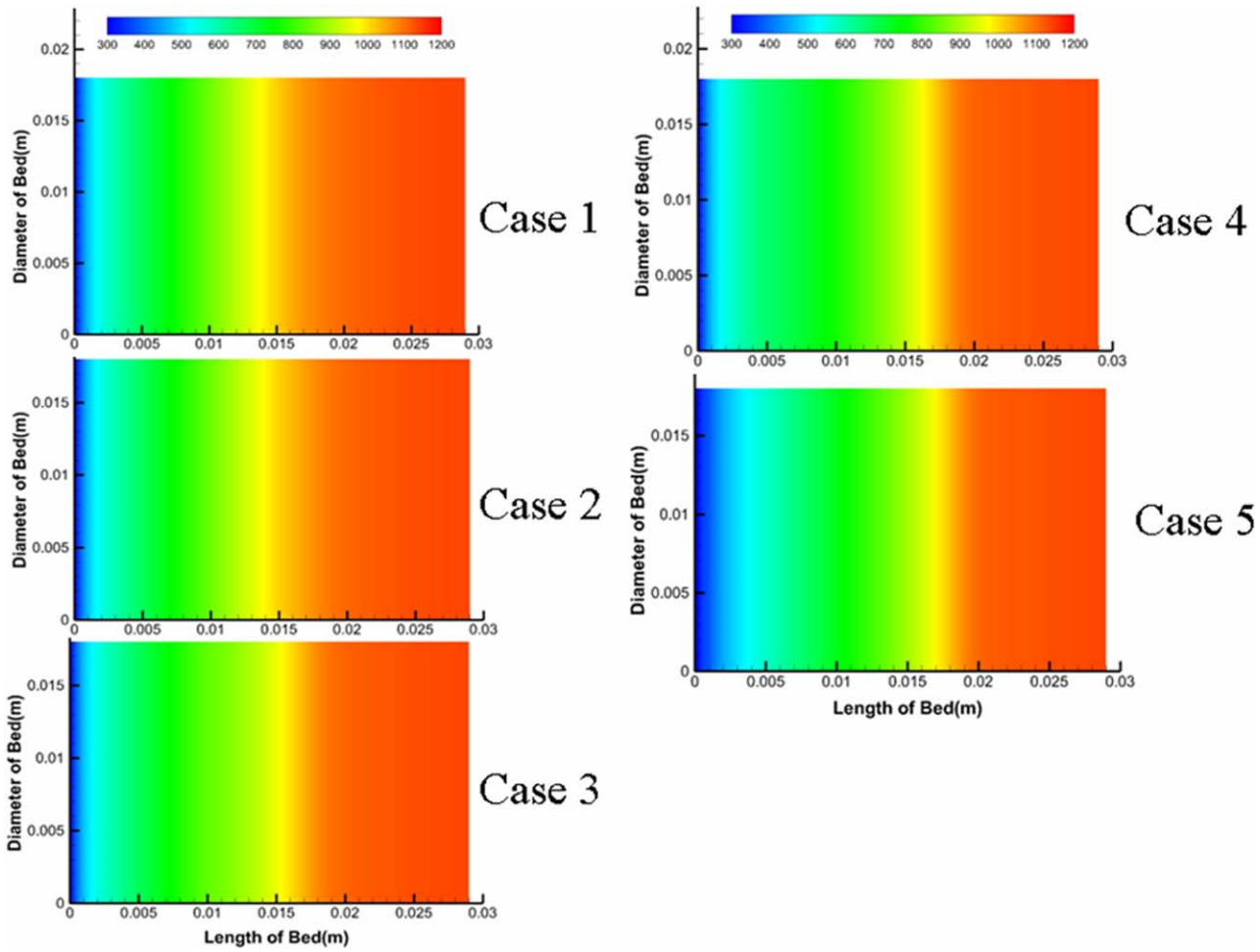

Figure 15. Distributions of the mixture temperature with various packing structures.

[Color figure can be viewed in the online issue, which is available at wileyonlinelibrary.com.]

calculated based on the rate of gas-liquid heat transfer as represented in Eq. 21, is controlled by the droplet burning in the high temperature gas phase. Due to the limitations of the gas-liquid and the liquid-solid heat transfer, the chemical energy released by the hydrazine decomposition reaction is not fully used to vaporize the liquid droplet, which explains for overestimating the liquid vaporization based on the Kesten's and Zhou's models, as shown in Figures 3–5.

In developing monopropellant thruster systems, researchers often reduce the catalyst diameter to improve the reaction rate of hydrazine catalytic decomposition reaction rate, but this reduction also leads to high flow resistance. Near the entrance of the packed bed, chemical energy needs to be released as fast as possible to vaporize the liquid droplet by the catalytic decomposition reaction of hydrazine, so selecting a small catalyst diameter favors improving the reaction rate and does not lead to high flow resistances because of the relative low fluid velocity, which is confirmed in Figures 11, 14, and 15. As the reaction proceeds and the hydrazine is fully depleted, a great deal of high-temperature gas products form, and the fluid velocity increases in the back of the packed bed, where using relatively bigger catalysts can decrease the packed-bed pressure drop. In addition, the main reaction occurring in the back of the packed bed is the catalytic decomposition of ammonia, which is dominated by the c intrinsic chemical reaction kinetics, so the effect of the catalyst particle size on the reaction rate in this region can be ignored. Therefore, the requirements of a high reaction rate and a low pressure drop across the packed bed can be simultaneously met using small particle size catalysts near the entrance of the packed bed and relatively larger catalysts in the back of packed bed.

The liquid propellant catalytic decomposition in the packed bed is distinguished from burning in the free space by the packed catalyst. Due to the thermal conductivity and the radiation of catalyst and the dispersion of the gas phase from the packed catalyst,[46] the catalyst can be used not only to decompose the propellant vapor but also to promote the stability of the thruster system. As much energy as possible is needed in the front of the packed bed to vaporize the liquid propellant, but most of chemical energy in the back of the packed bed is directly used to heat the catalyst and gas-phase products. Provided that the energy in the back of the packed bed can be efficiently transferred to the low-temperature region near the entrance by adjusting the catalyst properties, the packing structures or other parameters of packed bed, the rate of liquid vaporization can be improved, and the system temperature in the back of the packed bed can be reduced, so the catalyst life in the high-temperature region can be prolonged. This work has required extensive experimental testing in the past, but it is possible to enhance the effectiveness of such an experimental program by the mathematical model developed in this article.

Conclusions

A general model for liquid monopropellant decomposition with the simultaneous evaporation of liquid droplets in a packed bed is developed, taking gas-solid mass transfer and mass and heat conservation for mixtures or solid catalysts into account. In this model, the rate of the liquid droplet evaporation in porous media is obtained by calculating the gas-liquid mass and heat transfer or the liquid-solid heat transfer under the different conditions. An experiment studying hydrazine decomposition in the packed bed is used to validate the developed model, and there are good agreements between the theoretical predication and experimental results of the axial distribution of the gas mixture temperature. Based on the above discussions, the main conclusions can be summarized as follows:

1. Ignoring transport limitations or liquid evaporation effects, such as in the Kesten's and Zhou's models, overestimate the rate of liquid hydrazine vaporization and cannot obtain satisfactory prediction results for the axial distribution of the mixture temperature.

2. In the liquid hydrazine decomposition process in the packed bed, the catalytic decomposition of hydrazine is mainly dominated by the intrapartice diffusion of the reactants, and the ammonia decomposition reaction is determined by the intrinsic chemical reaction kinetics. In addition, the hydrazine catalytic decomposition reaction, which is three times faster than the homogeneous decomposition reaction of hydrazine and ammonia, dominates the decomposition process of liquid hydrazine in the packed bed.

3. In designing the packed bed for a thruster system, using small particle size catalysts near the entrance can accelerate the rate of liquid hydrazine vaporization, shorten the length of the gas-liquid coexistence region and broaden the operational range. However, if the length of packing in the bed with the small-particle size catalysts exceeds a certain value or enters the high-fluid velocity region in the back of packed bed, the pressure drop increase. Based on the theoretical method developed in this article, the appropriate catalyst size and the relevant packing length can be theoretically predicted.

4. Due to the heat conductivity and the radiation of the solid catalyst, energy can be transferred from the high-temperature region at the back of packed bed to low-temperature region near the entrance. This ability of balancing the energy from the porous media favors promoting the liquid hydrazine vaporization and stabilizing the performance of the liquid hydrazine decomposition in the packed bed.

Acknowledgments

The author is grateful to the supports on this work from the National Natural Science Foundation of China under Grant No. 21076211 and No. 21206159.

Notation

$c^{b}_{H_2}$ = hydrogen concentration in bulk phase, mol m^{-3}
$c^{s}_{H_2}$ = hydrogen concentration on the surface of catalyst, mol m^{-3}
$c^{b}_{N_2H_4}$ = hydrazine concentration in bulk phase, mol m^{-3}
$c^{s}_{N_2H_4}$ = hydrazine concentration on the surface of catalyst, mol m^{-3}
$c^{b}_{NH_3}$ = ammonia concentration in bulk phase, mol m^{-3}
$c^{s}_{NH_3}$ = ammonia concentration on the surface of catalyst, mol m^{-3}
$c^{*}_{N_2H_4}$ = concentration of hydrazine saturated steam at the relevant temperature, mol m^{-3}
$c_{p,m}$ = heat capacity of mixture, J kg^{-1} k^{-1}
d_c = catalyst diameter, m
d_p = liquid droplet diameter, m
D_{AB} = mass diffusion coefficient of binary mixture A and B, m^2 s^{-1}
D_{H_2} = effective diffusion coefficient for hydrogen, m^2 s^{-1}
$D_{N_2H_4}$ = effective diffusion coefficient for hydrazine, m^2 s^{-1}
D_{NH_3} = effective diffusion coefficient for ammonia, m^2 s^{-1}
D_{N_2} = effective diffusion coefficient for nitrogen, m^2 s^{-1}
h_g = enthalpy of gas, W kg^{-1} K^{-1}
h_{fg} = liquid hydrazine evaporation latent heat, J kg^{-1}
h_L = enthalpy of liquid, W kg^{-1} K^{-1}
k^{e}_{s} = effective conductivity of packed bed, W K^{-1} m^{-1}
$k^{N_2H_4}_{g,s}$ = mass-transfer coefficient for gas hydrazine between gas and solid, m s^{-1}
$k^{N_2H_4}_{g,s}$ = mass-transfer coefficient for ammonia between gas and solid, m s^{-1}
$k_{g,L}$ = mass transfer between gas and liquid, m s^{-1}
k_{rs} = heat-transfer coefficient for the thermal radiation, solid surface to solid surface, w m^{-2} K^{-1}
k_{rv} = heat-transfer coefficient for the thermal radiation, void space to void space, w m^{-2} K^{-1}
M_A = molecular weight for substance A, g mol^{-1}
M_B = molecular weight for substance B, g mol^{-1}
$m_{g,L}$ = mass exchange between liquid and gas, kg m^{-3}
M_m = mixture average molecular weight, g mol^{-1}
M_{H_2} = hydrogen molecular weight, g mol^{-1}
M_{N_2} = nitrogen molecular weight, g mol^{-1}
$M_{N_2H_4}$ = hydrazine molecular weight, g mol^{-1}
M_{NH_3} = ammonia molecular weight, g mol^{-1}
n = number of contact points on a semispherical surface of one solid particle
p = pressure of mixture, Pa
P^{A}_{c} = critical pressure of substance A, Pa
$q_{s,L}$ = heat flux between liquid and solid, J m^{-2}
R = gas constant, J mol^{-1} K^{-1}
$R^{N_2H_4}_{het}$ = rate of heterogeneous decomposition vapor hydrazine, mol, m^{-3} s^{-1}
$R^{N_2H_4}_{hom}$ = rate of homogeneous decomposition vapor hydrazine, mol, m^{-3} s^{-1}
$R^{NH_3}_{het}$ = rate of heterogeneous decomposition ammonia, mol, m^{-3} s^{-1}
S_M = momentum sink vector due to the packed bed, N m^{-3}
T_b = liquid hydrazine boiling temperature, K
T^{A}_{c} = critical temperature of substance A, K
T_m = mixture temperature, K
T_s = solid temperature, K
T^{*} = reference temperature, K
U_m = superficial velocity of mixture, m s^{-1}
u_m = mixture velocity, m s^{-1}
x_i = mole fraction of the ith pure gas
y_i = mass fraction of the ith pure components
Y_{g,N_2H_4} = mass fraction of hydrazine in gas mixture
Y_{g,NH_3} = mass fraction of ammonia in gas mixture
Y_{g,H_2} = mass fraction of hydrogen in gas mixture
Y_{g,N_2} = mass fraction of nitrogen in gas mixture

Greek letters

α = collision probability for liquid droplet and solid surface
$\alpha_{m,s}$ = heat-transfer coefficient between mixture and solid, W K^{-1} m^{-2}
$\alpha_{s,L}$ = heat-transfer coefficient between liquid and solid, W K^{-1} m^{-2}
β = empirical parameter
ε_A = characteristic energy of molecules A
ε_b = porosity of packed bed
ε_c = porosity of catalyst
ε_g = gas viodage
ε_L = liquid viodage
ε_r = emissivity of catalyst solid
η_{vap} = effectiveness factor of evaporation
$\eta_{N_2H_4}$ = effectiveness factor of intraparticle diffusion for hydrazine heterogeneous decomposition
η_{NH_3} = effectiveness factor of intraparticle diffusion for ammonia heterogeneous decomposition
θ_0 = angle corresponding to boundary of heat flow area for one contact point, radians
κ = dimensionless parameters $= \frac{k_s}{k_g}$
λ_d = thermal conductivity of mixture due to the dispersion of packed bed, W K^{-1} m^{-1}
$\lambda_{g,i}$ = thermal conductivity of the ith pure gas, W K^{-1} m^{-1}
$\lambda^{*}_{g,i}$ = thermal conductivity of the ith pure gas at the reference temperature, W K^{-1} m^{-1}

λ_m = thermal conductivity of mixture, W K^{-1} m^{-1}
λ_s = thermal conductivity of porous catalyst, W K^{-1} m^{-1}
$\lambda_{s,i}$ = thermal conductivity of ith component pure solid, W K^{-1} m^{-1}
$\lambda_{s,m}$ = thermal conductivity of solid mixture, W K^{-1} m^{-1}
μ_g = viscosity of gas, Pa s
μ_L = viscosity of liquid, Pa s
μ_m = viscosity of mixture, Pa s
ξ = empirical parameter
ρ_g = gas density, kg m^{-3}
ρ_L = liquid density, kg m^{-3}
ρ_m = mixture density, kg m^{-3}
σ = Stephan-Boltzmann constant, w m^{-2} K^{-4}
σ_A = characteristic diameter of molecules A, m
$\Delta H_r^{N_2H_4}$ = enthalpy of hydrazine decomposition reaction, J mol^{-1}
$\Delta H_r^{NH_3}$ = enthalpy of ammonia decomposition reaction, J mol^{-1}

Dimensionless number

Pe = dimensionless Peclect number $= \frac{u_m d_c}{\lambda_g}$
Sh = dimensionless Sherwood number $= \frac{k_{g,L} dp}{D_{N_2H_4}}$
Stk = dimensionless stokes number $= \frac{\rho_L d_p^2 u_m}{36 \mu_m d_s}$
ϕ_i = dimensionless Thiele module for the ith heterogeneous reaction $= \frac{d_c}{6}\sqrt{\frac{k_{het}^i}{D_i^e}}$
Ω_{AB} = dimensionless quantity (defined as a function of the dimensionless temperaturekT/ε_{AB})

Subscripts and superscripts

b = packed bed
c = catalyst
g = gas phase
H_2 = hydrogen
m = mixture
L = liquid phase
N_2H_4 = hydrazine
NH_3 = ammonia
N_2 = nitrogen
s = solid

Literature Cited

1. Davis NS, Keefe JH. Concentrated hydrogen peroxide as a propellant. *Ind Eng Chem*. 1956;48:745–748.
2. Davis DD, Dee LA, Greene B, Hornung SD, McClure MB, Rathgeber KA. Fire, explosion, compatibility and safety hazards of hydrogen peroxide. NASA Technical Memorandum TM-2004-213151, NASA Johson Space Center White Sand Test Facility, 2005.
3. Plumlee D, Steciak J, Moll A. Development and simulation of an embedded hydrogen peroxide catalyst chamber in low-temperature co-fired ceramics. *Int J Appl Ceram Technol*. 2007;5:406–414.
4. Gibbon D, Paul M, Jolley P. Energetic green propulsion for small spacecraft, AIAA Paper 2001–3247, Utah, 2001.
5. Amri R, Gibbon D. In orbit performance of butane propulsion system. *Adv Space Res*. 2012;49:648–654.
6. Amri R, Gibbon D, Rezougc T. The design, development and test of one newton hydrogen peroxide monopropellant thruster. *Aerosp Sci Technol*. 2013;25:266–272.
7. Krejci D, Woschnak A, Scharlemann C, Ponweiser K. Structural impact of honeycomb catalysts on hydrogen peroxide decomposition for micro propulsion. *Chem Eng Res Des*. 2012;90:2302–2315.
8. Patel KD, Bartsch MS, McCrink MH, Olsen JS, Mosier BP, Crocker RW. Electrokinetic pumping of liquid propellants for small satellite microthruster applications. *Sens Actuators B*. 2008;132:461–470.
9. An SY, Jo S, Wee J, HosungYoon H. Preliminary flight test of hydrogen peroxide retro-propulsion module. *Acta Astronaut*. 2010;67:605–612.
10. Zheng MY, Chen XW, Cheng RH, Li N, Sun J, Wang XD, Zhang T. Catalytic decomposition of hydrazine on iron nitride catalysts. *Catal Commun*. 2007;7:187–191.
11. Cheng RH, Shu YY, Zheng MY, Li L, Sun J, Wang XD, Zhang T. Molybdenum phosphide, a new hydrazine decomposition catalyst: microcalorimetry and FTIR studies. *J Catal*. 2007;249(22):397–400.
12. Wang HX, Geng JY, Chen X, Pan WX. Numerical simulation of a low-power hydrazine arcjet thruster. *Phys Proc*. 2012;32:732–742.
13. Hwang CH, Baek SW, Cho SJ. Experimental investigation of decomposition and evaporation characteristics of HAN-based monopropellants. *Combust Flame*. 2014;161:1109–1116.
14. Amrousse R, Keiichi Hori K, Fetimi W, Kamal Farhat K. HAN and ADN as liquid ionic monopropellants: thermal and catalytic decomposition processes. *Appl Catal B: Environ*. 2012;127:121–128.
15. Amrousse R, Katsumi T, Niboshi Y, Azuma N, Bachar A, Hori K. Performance and deactivation of Ir-based catalyst during hydroxylammonium nitrate catalytic decomposition. *Appl Catal A: Gen*. 2013;452:64–68.
16. Courtheóux L, Amariei D, Sylvie Rossignol S, Kappenstein C. Thermal and catalytic decomposition of HNF and HAN liquid ionic as propellants. *Appl Catal B: Environ*. 2006;62:217–225.
17. Anflo K, Möllerberg R. Flight demonstration of new thruster and green propellant technology on the PRISMA satellite. *Acta Astronaut*. 2009;65:1238–1249.
18. Gohardani AS, Stanojev J, Demairé A, Anflo K, Persson M, Wingborg N, Nilsson C. Green space propulsion: opportunities and prospects. *Prog Aerosp Sci*. 2014;71:128–149.
19. Liu LJ, Wei CY, Guo YY, Rogers WJ, Mannan MS, Hydroxylamine nitrate self-catalytic kinetics study with adiabatic calorimetry. *J Hazard Mater*. 2009;162:1217–1222.
20. van der Heijden AEDM, Leeuwenburgh AB. HNF/HTPB propellants: influence of HNF particle size on ballistic properties. *Combust Flame*. 2009;156:1359–1364.
21. Pandit AV, Kumar A, Srinivasa Rao G, Kedarnath C, Srihari R and Ranade VV. Modeling of liquid propellant combustion chamber. *Chem Eng J*. 2012;207:151–166.
22. Pandit AV, Kumar A, Srinivasa Rao G, Kedarnath C, Srihari R and Ranade VV. Decomposition of solid propellants in a combustion chamber. *Adv Chem Eng Res*. 2012;1:8–17.
23. Kesten AS. Analytical study of catalytic reactors for hydrazine decomposition. East Hartford: Annual Progress Report NO. F910461-12 NASA United Aircraft Research Laboratories, 1967.
24. Hwang CH, Lee SN, Baek SW, Han CY, Kim SK, Yu MJ. Effects of catalyst bed failure on thermo chemical phenomena for a hydrazine monopropellant thruster using Ir/Al2O3 catalysts. *Ind Eng Chem Res*. 2012;51:5382–5393.
25. Shankar V, Anantha Ram K, Bhaskaran KA. Prediction of the concentration of hydrazine decomposition products along a granular catalytic bed. *Acta Astronaut*. 1984;11:287–299.
26. Urrutia JL, Linan A, Crespo A, Fraga E. Development of an analytical model of hydrazine decomposition motors. Spain: ESTEC Contract 1121/70 AA, Instituto Nacional de Tecnia Aerospacial "Esteban Terradas" Madrid, 1967.
27. Wehinger GD, Eppinger T, Kraume M. Fluidic effects on kinetic parameter estimation in Lab-scale catalysis testinga critical evaluation based on computaional fluid dynamics. *Chem Eng Sci*. 2014;111:220–230.
28. Jaramaz S, Micković D, Elek P. Two-phase flows in gun barrel: Theoretical and experimental studies. *Int J Multiphase Flow*. 2011; 37:475–487.
29. Zhang T, Li GX, Yu YS, Sun ZY, Wang M, Chen J. Numerical simulation of ammonium dinitramide(ADN)-based non-toxic aerospace propellant decomposition and combustion in a monopropellant thruster. *Energy Conversion Manag*. 2014;87:965–974.
30. Zhou X, Hitt DL. Numerical modeling of monopropellant decomposition in a Micro-Catalyst bed. AIAA Paper 2005-5033, California, 2005.
31. Mujeebu MA, Abdullah MZ, Mohamad AA, Bakar MZA. Trends in modeling of porous media. *Prog Energy Combust Sci*. 2010;36:627–650.
32. Plaud M, Gallier S, Morel M. Simulations of heterogeneous propellant combustion: Effect of particle orientation and shape. In: Proceedings of the Combustion Institute. In press.
33. Thakre P, Duan Y, Yang V. Modeling of ammonium dinitramide (ADN) monopropellant combustion with coupled condensed and gas phase kinetics. *Combust Flame*. 2014;161:347–362.
34. Amri R, Rezoug T. Numerical study of liquid propellants combustion for space applications. *Acta Astronaut*. 2011;69:485–498.
35. Zaseck CR, Son SF, Pourpoint TL. Combustion of micron-aluminum and hydrogen peroxide propellants. *Combust Flame*. 2013;160:184–190.
36. Martynenko VV, Echigo R, Yoshida H. Mathematical model of sefsustaining combustion in inert porous medium with phase change under complex heat transfer. *Int J Heat Mass Transfer*. 1998;41: 117–126.
37. Turns SR. *An Introduction to Combustion: Concepts and Applications*, 2nd ed. New York: McGraw-Hill Companies, 2000.
38. Buyevich YA, Mankevich VN. Interaction of a dilute mist flow with a hot body. *Int J Heat Mass Transfer*. 1995;38:731–744.
39. Rohsenow WM, Ganich EN. Dispersed flow heat transfer. *Int J Heat Mass Transfer*. 1977;20:855–866.

40. Eberstein IJ, Glassman I. The gas phase decomposition of hydrazine and its methyl derivations. In: *The Tenth Symposium (International) on Combustion*, Pittsburgh, the Combustion Institute, 1965:365–374.
41. Mchale ET, Knox BE, Palmer HB. Determination of the decomposition kinetics of hydrazine using a single-pulse shock tube. In: *The Tenth Symposium (International) on Combustion*, Pittsburgh, the Combustion Institute, 1965:341–351.
42. Melton CE, Emmett PH. Transient species observed in the catalyzed decomposition of ammonia. *J Phys Chem.* 1964;68:3318–3324.
43. Logan SR, Kemball C. The catalytic decompostion of ammonia on evaporated metal films. *Trans Faraday Soc.* 1960;56:144–153.
44. Levenspiel O. *Chemical Reaction Engineering*, 3rd ed. New York: Wiley, 1999.
45. Bird BR, Stewart WE, Lightfoot EN. *Transport Phenomena*, 2nd ed. New York: Wiley, 2002.
46. Aris R, Amundson NR. Some remarks on longitudinal mixing or diffusion in fixed beds. *AIChE J*. 1957;3:280–282.
47. Gonzo EE. Estimating correlations for the effective thermal conductivity of granular materials. *Chem Eng J*. 2002;90:299–302.
48. Kuni D, Smith JM. Heat transfer characteristics of porous rocks. *AIChE J*. 1960;6:71–78.
49. Mujeebu A, Abdullah MZ, Abu Bakar MZ, Mohamad AA, Abdullah MK. A review of investigations on liquid fuel combustion in porous inert media. *Prog Energy Combust Sci*. 2009;35:216–230.

Manuscript received June 26, 2014, and revision received Oct. 19, 2014.